




Electrolyte Effect on Photoetching of Gallium Nitride

Huiqiang Liang^{1,2} · Zhenghao Wei^{1,2} · Jiongchong Fang^{1,2} · Yanming Li³ · Changli Li³ · Zhirun Xie⁴ · Yun Hau Ng^{4,5} · Guosong Zeng^{1,2,6} 

Received: 28 December 2023 / Revised: 23 January 2024 / Accepted: 28 January 2024
© The Author(s) 2024

Abstract

The limited material removal rate of conventional chemical mechanical polishing (CMP) significantly hinders the fabrication efficiency and surface quality, thereby preventing the development of gallium nitride (GaN)-based devices. Moreover, the incorporation of photoelectrochemistry in CMP has garnered increasing attention because of its potential to enhance the quality and efficiency of the GaN process. However, a considerable gap still exists in the comprehensive understanding of the specific photoelectrochemical (PEC) behavior of GaN. Here, we report the influence of the electrolyte on the PEC etching of GaN. Various acids and bases were tested, with their pH being carefully adjusted. The concentrations of the cations and anions were also examined. The results showed that photocorrosion/photoetching was more pronounced in sulfuric acid, phosphoric acid, and nitric acid environments than in alkaline environments, but it was less pronounced in hydrochloric acid. Furthermore, the effects of pH and anion concentration on photoetching were investigated, and the results revealed that photoetching in acidic environments weakened with increasing pH levels and diminished with increasing sulfate concentration. The underlying reasons contributing to this observation were explored. These findings provide ideas for improving the photoetching efficiency of GaN, thereby enriching the photoelectrochemical mechanical polishing (PECMP) technology of GaN.

Highlights

1. The impact of various anion and cation species, pH values, and ion concentrations on the PEC behavior of GaN was investigated.
2. The differences in the photoetching of GaN under various solution environments were analyzed.

Keywords GaN · Photoelectrochemistry · Photoetching · pH

Huiqiang Liang and Zhenghao Wei have contributed equally to this paper.

✉ Guosong Zeng
zenggs@sustech.edu.cn

¹ Shenzhen Key Laboratory of Intelligent Robotics and Flexible Manufacturing Systems, Southern University of Science and Technology, Shenzhen 518055, People's Republic of China

² Department of Mechanical and Energy Engineering, Southern University of Science and Technology, Shenzhen 518055, People's Republic of China

³ School of Materials, Sun Yat-Sen University, Guangzhou 510275, People's Republic of China

⁴ School of Energy and Environment, City University of Hong Kong, Kowloon 999077, Hong Kong SAR, People's Republic of China

⁵ City University of Hong Kong Shenzhen Research Institute, Shenzhen Hi-Tech Industrial Park, Nanshan District, Shenzhen 518000, People's Republic of China

⁶ SUSTech Energy Institute for Carbon Neutrality, Southern University of Science and Technology, Shenzhen 518055, People's Republic of China

1 Introduction

With the rapid development of the information age, the demand for high-performance semiconductor devices is also growing [1–9]. Following the emergence and development of first-generation semiconductors (Si and Ge) and second-generation semiconductors (GaAs and InP), third-generation semiconductor gallium nitride (GaN) has attracted extensive attention because of its outstanding characteristics, such as a direct bandgap, high breakdown voltage, high electron mobility, high mechanical and chemical stability, and strong radiation resistance [1, 4, 10–13]. Given the aforementioned advantages, GaN has been widely used in diverse fields, such as aerospace, national defense, lighting, renewable energy, power electronics, and 5G communications [14–20]. To obtain excellent performance in GaN-based devices, it is better to conduct homoepitaxy of GaN to minimize the interfacial dislocation density [21, 22]. Therefore, a perfectly finished GaN substrate is of paramount importance for the subsequent epitaxy [23]. Currently, chemical mechanical polishing (CMP) is the primary processing technique for achieving globally planarized and damage-free semiconductor wafer surfaces [22, 24–26]. However, compared with silicon, GaN possesses notable hardness, brittleness, and chemical inertness [27, 28]. Therefore, the main challenges in employing conventional CMP to achieve ultra-precision polishing of GaN lie in its low material removal rate (MRR) and poor surface quality, which makes the GaN substrate fail to meet the practical demands of industrialization [29–32]. To address the aforementioned problems, other energy fields (e.g., magnetic fields, electric fields, and light fields) have been introduced on the basis of CMP to enhance the MRR and further improve the surface quality of GaN [30, 31, 33–37]. Compared with plasma-assisted polishing, magnetic field-assisted polishing, and ultrasonically assisted electrochemical mechanical polishing, photoelectrochemical mechanical polishing (PECMP) features a simple configuration; it inherits most of the CMP with the minimum modification of the current apparatus, leading to a cost-effective adaptation of conventional CMP equipment. Moreover, PECMP exhibits significant enhancements in both processing efficiency and quality, thus attracting increasing attention. Dong et al. developed a novel PECMP system and applied it to the polishing of GaN. They achieved a high MRR of up to 1.2 $\mu\text{m}/\text{h}$ and obtained an atomically smooth surface with a roughness of 0.067 nm over an area of $1 \times 1 \mu\text{m}^2$ [38]. Ou and his colleagues selected Au nanoparticles as the photocathode to facilitate the extraction of photogenerated electrons from GaN under light irradiation in the presence of an oxidizing agent, which is beneficial for GaN oxidation via photogenerated holes [39]. Qiao et al. found that during PECMP processing, the MRR of GaN was

determined by the oxidation of GaN, which correlated positively with the bias voltage and UV light intensity but negatively with the dislocation density of GaN [40].

CMP and PECMP mainly differ in the surface oxidation method. CMP employs oxidants such as H_2O_2 or KMnO_4 for surface oxidation [41–45], while PECMP can more effectively achieve this goal by introducing an external energy source (*i.e.*, UV light and bias voltage) to overcome the energy barrier of GaN oxidation. In the PECMP process, the GaN surface undergoes oxidation by photogenerated holes to form a softer oxide layer, which is subsequently removed by abrasives [39, 46]. Therefore, balancing the oxidation rate achieved via photoelectrochemistry and the oxide removal rate is a critical issue for advancing this novel polishing technique. However, studies have predominantly focused on the mechanical removal process, while the photoelectrochemical (PEC) process of GaN has received less attention. Several factors, including pH, applied bias, and illumination, significantly influence the PEC behavior of GaN. A systematic investigation into the roles of these factors will contribute to a more comprehensive understanding of the PECMP of GaN.

In this study, we performed PEC testing on GaN in various electrolytes with different concentrations and pH values. The PEC behavior and surface morphology (obtained via atomic force microscopy and scanning electron microscopy) were systematically analyzed and compared. The results showed that in an acidic environment, the relationship between photocurrent and photoetching highly depended on the anions, resulting in a severely corroded surface from nitric acid, sulfuric acid, and phosphoric acid but a sustained almost pristine-like surface with hydrochloric acid. The GaN tested under the alkaline solution showed a similar photocurrent but a barely corroded surface. Furthermore, the pH and ionic effects on the photoetching of GaN were investigated. This finding can elucidate the appropriate electrolyte selection for PECMP of GaN and serve as a testing model for the discovery of suitable solution for other semiconductor fabrications.

2 Materials and Methods

2.1 Specimen

Commercial GaN epilayers grown on sapphire substrates with a thickness of $\sim 4 \mu\text{m}$ (Shanghai GaNova Electronic Information Co., Ltd., China) were cleaved into the appropriate chips. Subsequently, the samples were sonicated in acetone, ethanol, and DI water for 5 min and then dried with N_2 . Finally, copper wires were connected to the samples using silver paste, and exposed copper wires and silver paste were isolated using epoxy resin to prevent contact with the electrolyte.

2.2 PEC Measurements

A 500 W Xe lamp (PLS-FX 300 HU, Beijing Perfectlight Technology Co., Ltd., China) with an AM 1.5G filter was used as the light source, and the light output was calibrated to 6 suns (600 mW cm^{-2}) using a power meter (PL-MW2000, Beijing Perfectlight Technology Co., Ltd., China). The PEC performance of GaN was evaluated in a three-electrode configuration using an electrochemical workstation (CHI760e, Shanghai Chenhua Instrument Co., Ltd., China). The reference electrodes in acidic and alkaline environments were saturated calomel (SCE) and Hg/HgO electrodes, respectively. A Pt piece was used as the counter electrode. In this study, all linear sweep voltammetry (LSV) measurements were conducted with anodic sweeping (*i.e.*, scanned toward the positive direction) at a rate of 50 mV s^{-1} , and chronoamperometry (CA) measurements lasted 15 min. In all cases, light irradiation came from the front side of the electrodes. All potentials reported in this work were against the reversible hydrogen electrode (RHE) and were obtained relative to the SCE or Hg/HgO reference electrode using the Nernst equation [47, 48]:

$$E_{\text{RHE}} = E_{\text{SCE}} + 0.0591\text{pH} + 0.1976\text{V (in acidic experiment)}$$

$$E_{\text{RHE}} = E_{\text{Hg/HgO}} + 0.0591\text{pH} + 0.098\text{V (in alkaline experiment)}$$

Unless specified otherwise, the pH values for all acidic and alkaline environments were 0 and 14, respectively. After the PEC experiments were completed, GaN was sonicated in acetone, ethanol, and DI water for 5 min and then dried with N_2 .

2.3 Atomic Force Microscopy and Scanning Electron Microscopy

The surface morphology of the pristine GaN and GaN after 15 min of CA measurements was characterized via atomic force microscopy (AFM, Bruker Dimension Icon, Bruker Co., Germany) and scanning electron microscopy (SEM, Apreo2 S Lovac, Thermo Fisher Scientific Brno s.r.o, Czechia). The equipped AFM tip, purchased from Bruker, consisted of a silicon tip on a nitride lever. The surface roughness (R_a) of the samples was measured via AFM within a scan area of $2 \mu\text{m} \times 2 \mu\text{m}$.

2.4 Inductively Coupled Plasma Mass Spectrometry

The electrolytes used for CA measurements were analyzed via inductively coupled plasma mass spectrometry (ICP-MS, Agilent 7700X, Agilent Technologies Co. Ltd., USA). Aqueous 2 wt% HNO_3 was used as the carrier solution to dilute

the analyzed samples. After CA tests, aqueous solutions of sulfuric, phosphoric, nitric, and hydrochloric acids, as well as sodium hydroxide and potassium hydroxide, were collected to identify gallium ion concentrations. The volume of all electrolytes used in the ICP-MS experiments was 80 mL.

2.5 In situ Raman Spectroscopy

In situ Raman experiments (DXR2xi, Thermo Fisher Scientific Inc., USA) were conducted in sulfuric acid at pH 0, with GaN serving as the working electrode and platinum wire acting as the counter and reference electrodes. The laser wavelength was 532 nm, and the exposure time was 10 s. To minimize the interference of visible stray light with Raman measurements, a ZWB2-type ultraviolet-transmitting optical filter was used.

2.6 X-ray Photoelectron Spectroscopy

The chemical compositions of the pristine surface and the surface subjected to a 15 min CA test in H_2SO_4 (pH 0) of GaN were analyzed via X-ray photoelectron spectroscopy (XPS, Escalab Xi+, Thermo Fisher Scientific Inc., USA). An Al $K\alpha$ X-ray source ($h\nu = 1,486.6 \text{ eV}$) and a spot size of $100 \mu\text{m}$ were employed for the detection of the core levels of the Ga 3d, N 1s, and O 1s regions. A pass energy of 20 eV was used for the narrow scan with a step size of 0.01 eV for each core level. The binding energy scales of all core levels were corrected to the N 1s of the Ga-N bond at 397.8 eV (Fig. S1).

3 Results and Discussion

3.1 PEC Testing in an Acidic Environment

To evaluate the effect of the electrolyte on the PEC behavior and the photoetching of GaN, we first tested GaN in different acids. Sulfuric acid, nitric acid, hydrochloric acid, and phosphoric acid were chosen as the electrolytes, and the testing conditions (applied bias, illumination intensity, total time for CA, pH, linear sweep voltammetry) were kept the same. Considering that GaN is a renowned material for PEC photoelectrode protection, we employed much higher radiation intensity to intensify the photoetching process; thus, the electrolyte effect could be distinguished more conveniently. First, the dark current under all circumstances could be neglected, as shown in Fig. S2, which excludes the dissolution and electrochemical degradation of GaN. Figure 1 compares the LSV and CA plots for different acidic solutions under 6-sun illumination. H_2SO_4 yielded the highest saturated photocurrent, and HNO_3 exhibited the lowest saturated

photocurrent, while H_3PO_4 showed the highest cathodic onset potential (Fig. 1a). We selected $V_{\text{RHE}} = 2.25$ V as the applied bias for all tests to guarantee that the CAs were conducted at the corresponding photocurrent steady states. Figure 1b shows a similar order of the photocurrent as the LSV plots, with H_2SO_4 exhibiting the highest performance, while HNO_3 shows the lowest performance. All cases except for HCl exhibited an increase in photocurrent, with H_2SO_4 exhibiting the most significant growth (0.39 to 0.48 mA/cm^2 , growth of 23%) and HNO_3 exhibiting the least growth (0.25 to 0.27 mA/cm^2 , growth of 8%). Such an increase in photocurrent can originate either from self-improving (referred to

as self-healing in some studies) [14, 49–51] or photocorrosion [52]. Therefore, the tested surfaces were analyzed via SEM and AFM to determine the origin of the increase in photocurrent. The pristine surface morphology is shown in Fig. 2a and Fig. S3. According to the SEM results (Figs. 2 and S4), various forms of photocorrosion occurred on the surface of GaN in H_2SO_4 , HNO_3 , and H_3PO_4 . In contrast, the HCl-tested surface remained almost intact. To study the size of corroded pits and Ra, we further investigated the surface morphology of GaN via AFM (Fig. S5). The corrosion/etching of the GaN surface exhibited the following sequence: $\text{H}_2\text{SO}_4 > \text{H}_3\text{PO}_4 > \text{HNO}_3 > \text{HCl}$, which is consistent with

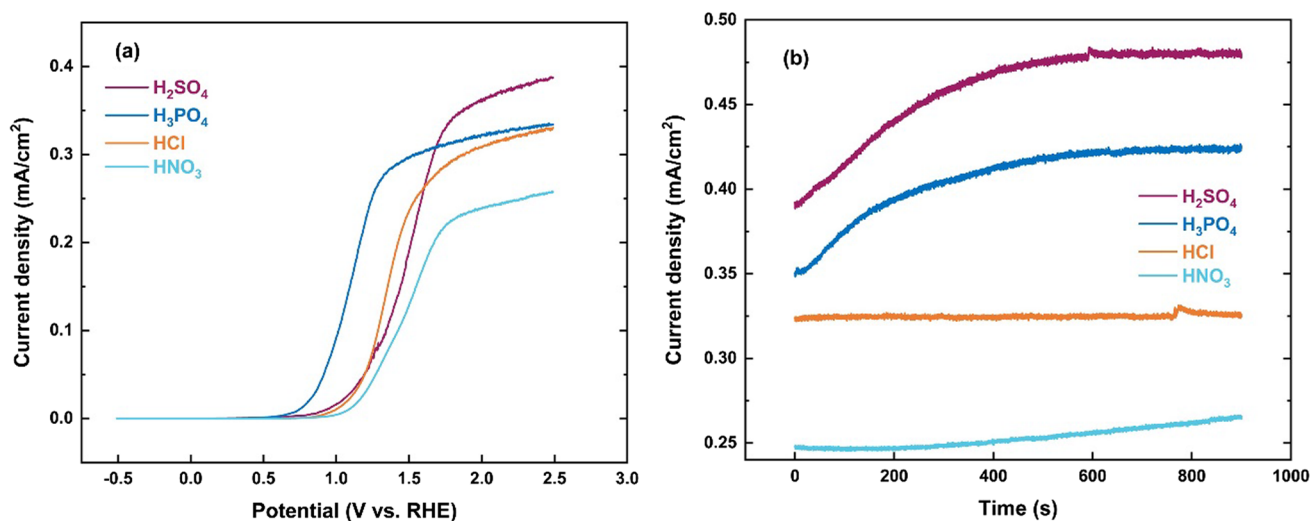


Fig. 1 a LSV curves of GaN under illumination in H_2SO_4 , H_3PO_4 , HNO_3 , and HCl at pH 0. b CA curves of GaN based on 2.25 V vs. RHE in H_2SO_4 , H_3PO_4 , HNO_3 , and HCl at pH 0

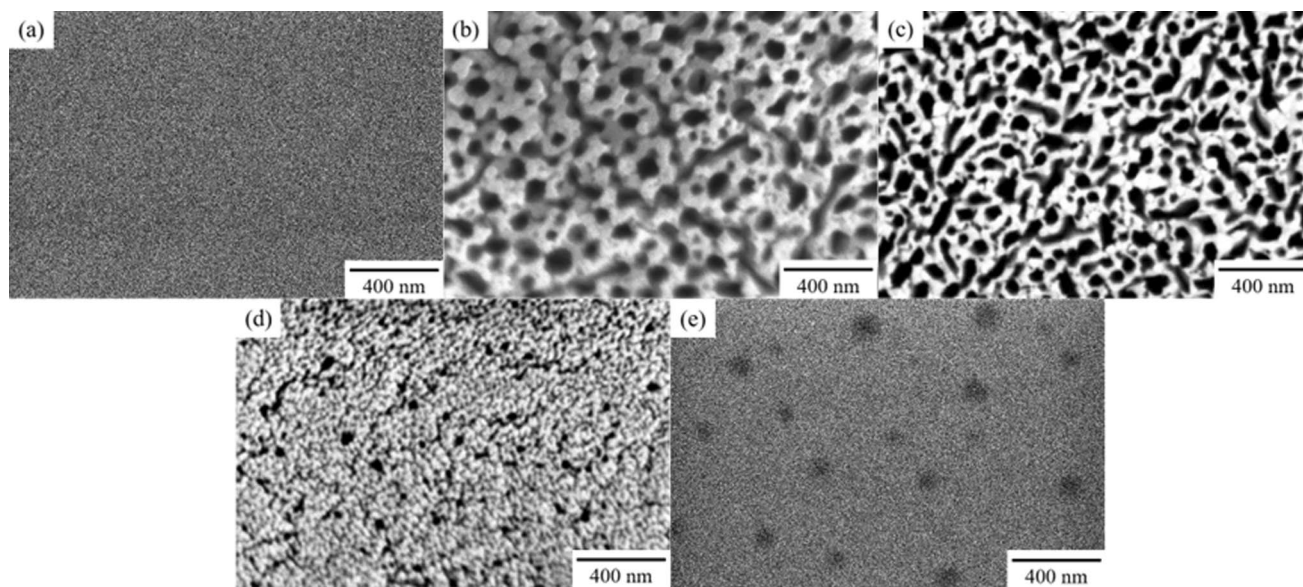
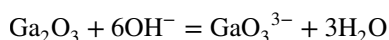
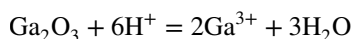
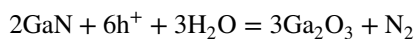


Fig. 2 SEM morphology images of a pristine GaN and GaN after CA tests in b H_2SO_4 , c H_3PO_4 , d HNO_3 , and e HCl at pH 0

the CA results, except for HNO_3 (Fig. 1b). Specifically, the H_2SO_4 -etched surface exhibited large pores and grain-like structures, while the HNO_3 -etched surface showed much tinier grain features compared with the H_2SO_4 case, with negligible pinholes afterward. The surface morphology measured via AFM aligned well with the SEM results. In addition to characterizing the surface morphology, we further elucidated the findings through the analysis of Ra and the Ga ions contained in the electrolyte after CA tests. The tested H_2SO_4 solution contained significant Ga ions, whereas the Ga ions were barely visible in the HCl solution (Fig. 3). Thus, we speculate that the increasing in photocurrent is strongly correlated with surface corrosion/etching, in which the corrosion of GaN highly depends on the types of anions used during the PEC process. Extensive research has been conducted on the photocorrosion (or photoetching) process in GaN during PEC processes [30, 53–56]:



Some studies have experimentally observed the phenomenon of the photocorrosion of GaN in acidic experiments [53, 57–59]. Through Gibbs free energy calculations, Chen's team revealed that GaN exhibited a higher oxidation potential in acidic environments at pH 0 compared with the oxidation potential of water, which confirms the thermodynamically feasible occurrence of photocorrosion in GaN under illumination at acidic conditions [60]. Nandjou et al. reported similar conclusions

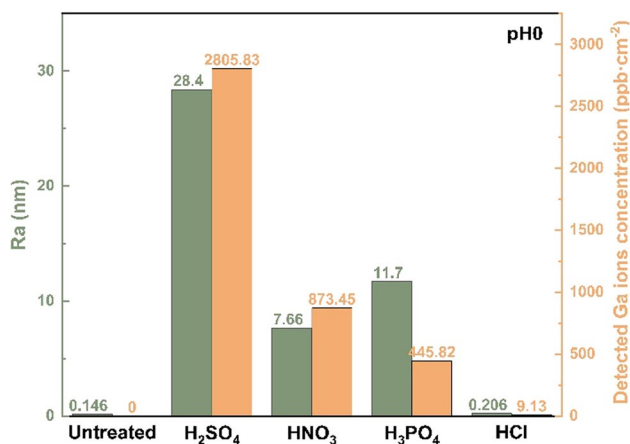


Fig. 3 Ra of the untreated GaN and GaN after CA tests in H_2SO_4 , H_3PO_4 , HNO_3 , and HCl at pH 0, and the concentration of Ga ions measured via ICP-MS after CA tests in the same solutions

[61]. The authors experimentally and theoretically confirmed that GaN underwent photocorrosion in acidic environments. In this work, we employed in situ Raman spectroscopy to investigate the changes in GaN during the CA test in the presence of H_2SO_4 . In situ Raman analysis under PEC testing conditions was performed within a self-constructed PEC cell (Fig. 4a), and the changes in surface composition of GaN during the CA test (Fig. S6) were tracked. Figure 4b illustrates the Raman spectra acquired in H_2SO_4 . The Raman peak at 417 cm^{-1} corresponded to the sapphire substrate [62–64], whereas the peaks at 570 and 735 cm^{-1} corresponded to GaN [62, 65, 66]. The appearance of the Raman peak of the sapphire is attributed to the longitudinal resolution of Raman imaging being $\sim 2\text{ }\mu\text{m}$, and GaN exhibited good light transmittance. If the Raman focus is not perfectly aligned with the surface of GaN, there is a possibility of acquiring a signal from the sapphire substrate instead. In H_2SO_4 , the minor shoulder located near 748 cm^{-1} belongs to gallium oxide during the CA test [67–69]. During the initial phases of the CA test in H_2SO_4 , gallium oxide progressively emerged and was sustained throughout subsequent reactions without an escalation in content. In contrast to other reactions in which the product concentration gradually increases, this phenomenon originates from a dynamic equilibrium between the oxidation of GaN by photogenerated holes, leading to the formation of gallium oxide, and the dissolution of gallium oxide by H_2SO_4 .

Considering that the in situ Raman spectroscopy has a relatively large detection limit and that the signal of oxide was quite weak for observation, some uncertainties existed. Therefore, XPS was applied to check the surface chemical composition before and after PEC testing. The O 1s from the etched surface showed a weaker O–Ga signal compared to the pristine GaN surface (Fig. 5), and both surfaces featured a similar amount of chemisorbed OH that bound to the oxide layer. Moreover, the Ga 3d peak was perfectly aligned with O 1s, and the etched surface also exhibited a weaker Ga–O signal. Given that the probing depth of XPS was only about a few nanometers of the topmost surface, and the total integrated area of the oxide peak from the etched surface was not much smaller than that of the pristine surface, the results further indicated that the etched surface was first oxidized and then quickly dissolved in the electrolyte.

Furthermore, the extent of photoetching significantly varied depending on the specific acid, and this variation was due to the influence of anions. In particular, photoetching in HCl was less severe than that in H_2SO_4 . This was due to the specific adsorption of Cl^- ions on the surface of the material, and photogenerated holes might preferentially oxidize Cl^- ions, thereby inhibiting the photocorrosion of semiconductors [70–75].

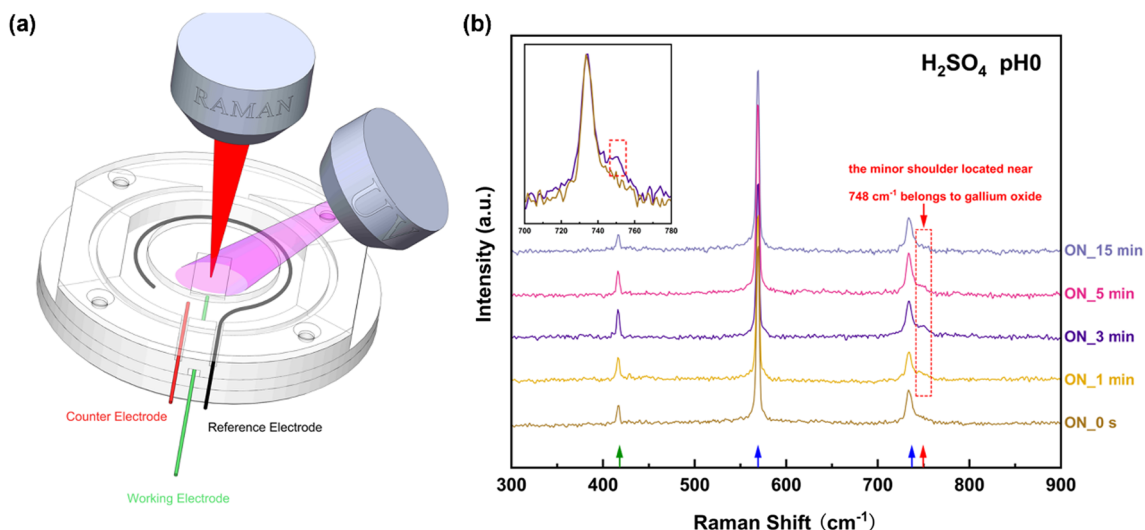


Fig. 4 **a** Schematic of the PEC cell used for in situ Raman PEC measurements. **b** In situ Raman spectroscopy results of the CA test in H_2SO_4 at pH 0. “ON_x min” refers to the x-th minute after the start

of the CA test. The inset is an enlarged image near the minor shoulder after normalization processing in “ON_3 min” and “ON_0 s”.

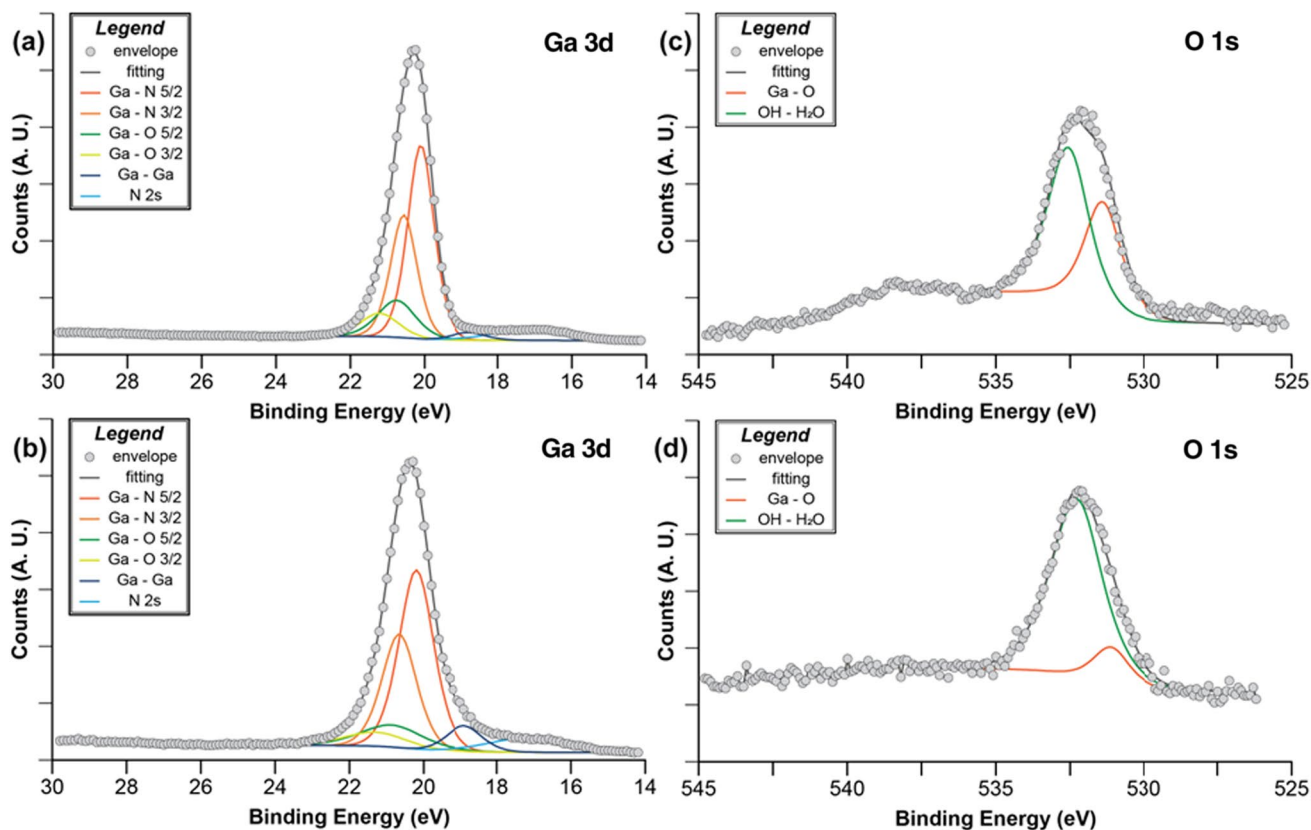


Fig. 5 Ga 3d XPS spectra of **a** pristine GaN surface and **b** GaN surface after the CA test in H_2SO_4 at pH 0. O 1s XPS spectra of **c** pristine GaN surface and **d** GaN surface after the CA test in H_2SO_4 at pH 0

To further examine the effect of the acid solution, different pH values (0, 1, 2, and 4) of H_2SO_4 were employed. The lower the pH value in an acidic environment, the

higher the photocurrent (Figs. 6a and S7), which resulted in much heavier corrosion of GaN (Figs. 6b and 7). Except for a slight decrease in photocurrent observed in the pH 4

environment (0.252 to 0.248 mA/cm², decrease of 1.6%), photocurrent significantly increased with decreasing pH (Fig. S7). Hill et al. revealed that as the pH of H₂SO₄ increased, the kinetics of oxygen evolution reaction (OER) improved [70]. This substantiates the notion that an elevated pH value improves hole transfer, thereby diminishing photoetching. The relationship between the pH value and the PEC behavior of GaN can be explained by thermodynamics. Figure 8 delineates the oxidation potential and reduction potential relative to the normal hydrogen electrode and vacuum level for a range of semiconductors in solution at pH 0. According to the Nernst equation [47, 48], when the pH value increased by 1, the oxygen

evolution potential increased by -0.0591 V. Therefore, as the pH value increased, more holes migrated to the interface to trigger OER, and fewer holes were available to oxidize GaN, resulting in weaker etching.

3.2 PEC Testing in an Alkaline Environment

For comparison, the photoetching of GaN was also tested in alkaline solutions (namely sodium hydroxide and potassium hydroxide) at pH 14. As can be seen in Figs. 9a and S8, the photocurrent from NaOH was higher than that from KOH, whereas the CA, unlike the acidic solution, showed a relatively stable photocurrent over a certain period of

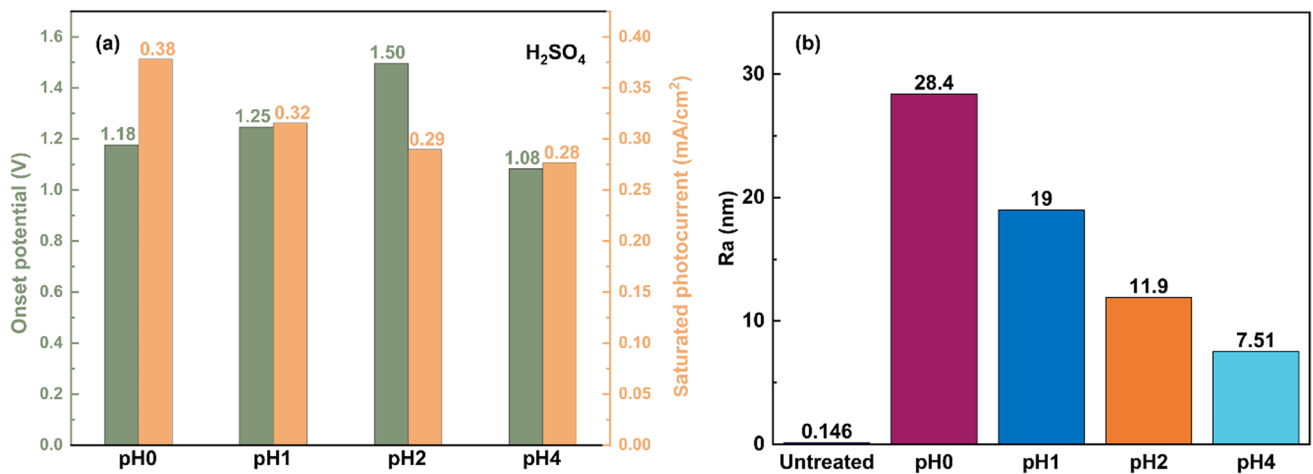


Fig. 6 **a** Onset potential and saturated photocurrent of GaN in H₂SO₄ at pH 0, 1, 2, and 4. **b** Ra of pristine GaN and GaN after CA tests in H₂SO₄ at pH 0, 1, 2, and 4, respectively

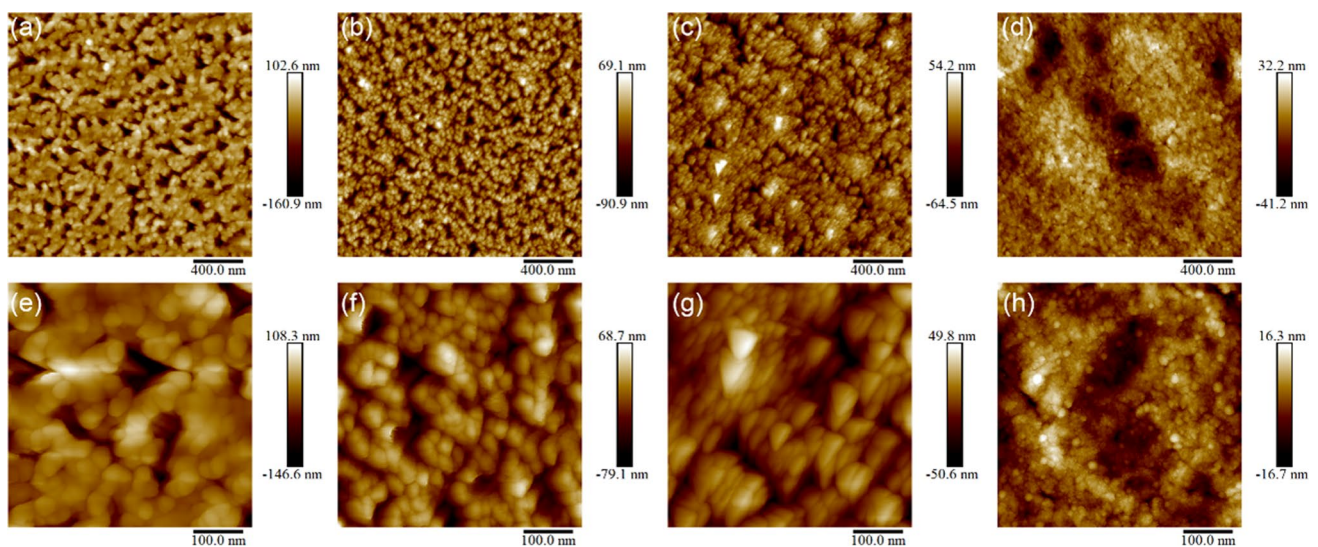


Fig. 7 **a–d** 2 μm -scale AFM images of GaN after CA tests in H₂SO₄ at pH 0, 1, 2, and 4, respectively. **e–h** 500 nm-scale AFM images corresponding to (**a–d**)

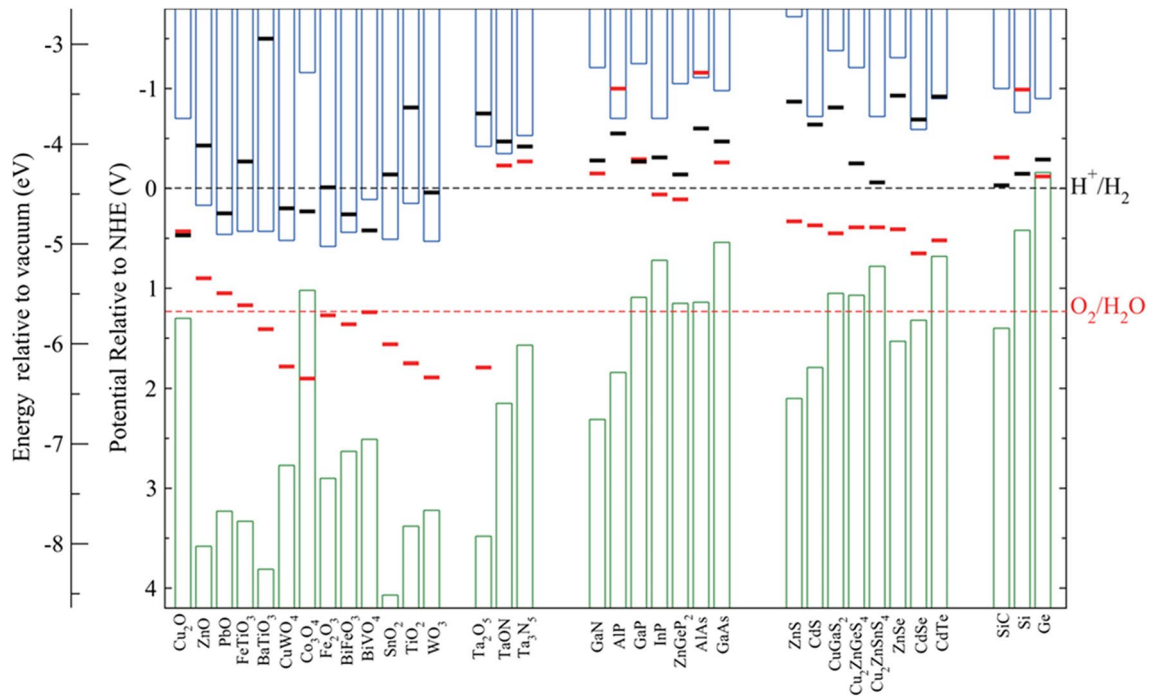


Fig. 8 Calculated oxidation potential (red bars) and reduction potential (black bars) relative to the normal hydrogen electrode and vacuum level for a series of semiconductors in solution at pH 0, ambient

temperature 298.15 K, and pressure 1 bar. The water redox potentials (dashed lines) and the valence (green columns) and conduction (blue columns) band edge positions at pH 0 are also plotted [60]

testing time. The surface morphology and Ra obtained via AFM showed that in an alkaline environment, etching barely occurred, with KOH presenting tiny pores, whereas NaOH exhibited an almost pristine-like surface after CA tests (Figs. 9b and 10). The Ga ions concentration measured via ICP–MS also validates this point (Fig. 9b). The milder photoetching of GaN in alkaline electrolytes also verifies our speculation that a higher pH corresponds to reduced photoetching.

The OER conventionally uses OH^- ions as its primary reactants in alkaline electrolytes [61, 76–78]. Because the ionic radius of K^+ is larger than that of Na^+ , when a KOH electrolyte is used, the large K^+ ions act as an impediment to the effective adsorption of OH^- ions onto the active sites of the GaN surface [79, 80]. This hindrance leads to the accumulation of a greater number of photogenerated holes, which in turn results in mild photoetching. In addition, Ding et al. employed density functional theory calculations and

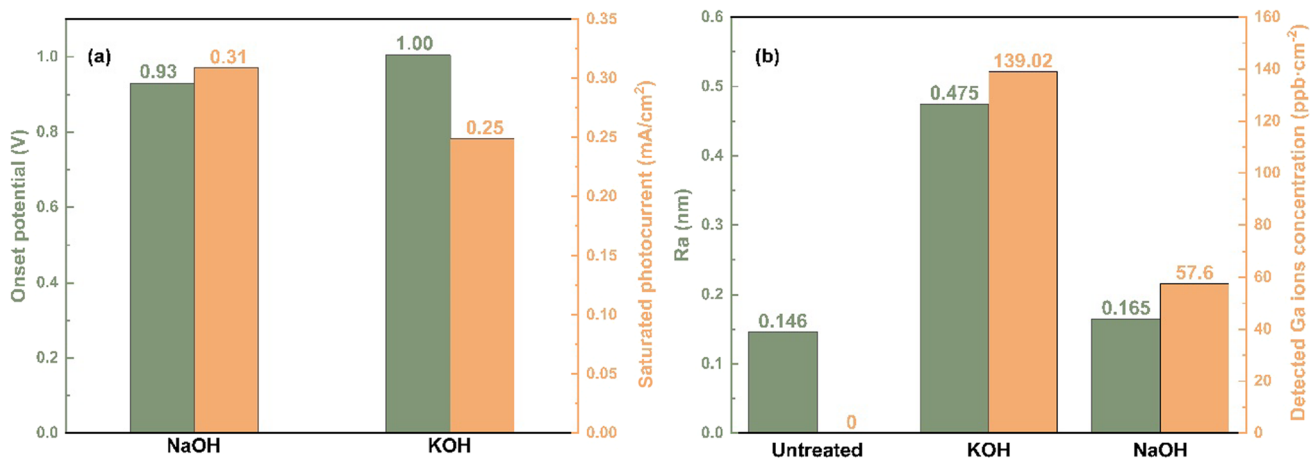


Fig. 9 **a** Onset potential and saturated photocurrent of GaN in NaOH and KOH at pH 14. **b** Ra of pristine GaN and GaN after CA tests in NaOH and KOH at pH 14, and the concentration of Ga ions measured via ICP–MS after CA tests in the same solutions

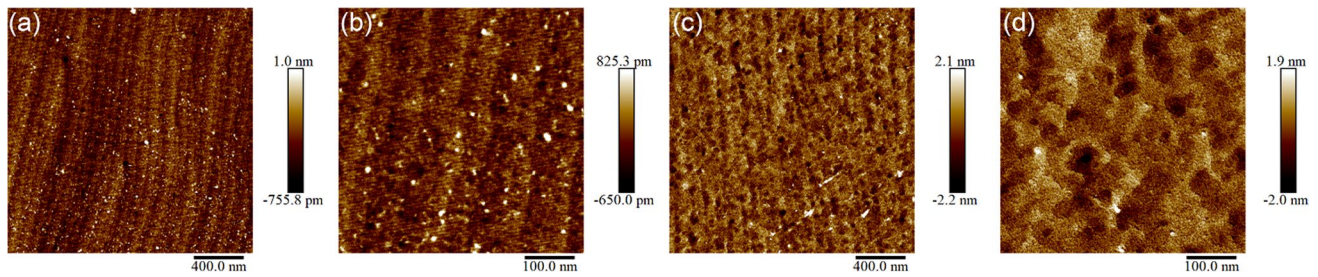


Fig. 10 a, c 2 μm -scale AFM images of GaN after CA tests in NaOH and KOH at pH 14, respectively. b, d 500 nm-scale AFM images corresponding to (a, c)

determined that hydrated sodium ions exhibited higher affinity to OH^- species on the electrode surface than potassium ions. This increased interaction resulted in the weakening of the O–H bond, thereby enhancing the OER. This led to a relatively reduced occurrence of photoetching [79]. In addition to the ion dimension, other factors such as ion conductivity (interface kinetics) and electrochemical activity might also contribute to this cation effect [81, 82].

3.3 Anionic Concentration Effect on the Photoetching of GaN

According to the ionic effect on GaN photoetching, H_2SO_4 exhibited the most significant impact on GaN. To further determine how this sulfate radically affected the stability of GaN, we conducted a PEC test of GaN in an acidic environment with various controlled SO_4^{2-} concentrations. Because NaOH had the mildest influence, sodium sulfate was used to adjust the concentration of SO_4^{2-} . As shown in Table 1 and Figs. S9 and 10, with the increase in the concentration of SO_4^{2-} , surface corrosion was greatly alleviated, photocurrent generation was reduced, fewer pores were generated, and surface roughness continually decreased.

Under PEC conditions, the oxidation of SO_4^{2-} or HSO_4^- ions, which tended to be adsorbed at the surface sites of semiconductor materials, expedited the transfer or consumption of photogenerated holes [70, 83–87]. This phenomenon contributed to the reduction in photoetching resulting from residual holes at the surface/interface.

Furthermore, the increased presence of SO_4^{2-} ions enhanced solution mass transfer and reduced interfacial impedance, thus further facilitating photogenerated holes transfer at the surface/interface [88, 89].

4 Conclusion

We systematically investigated the effect of electrolytes on GaN photoetching during the PEC process. Both acidic and alkaline electrolytes were used and compared, and various anions and cations were also investigated. The results revealed that the acids actively interacted with the GaN surface and led to a severely corroded surface, except for HCl. The peculiar behavior of HCl is attributed to the competition between surface corrosion and Cl_2/O_2 evolution. Furthermore, the alkaline electrolytes induced insubstantial damage to GaN. The GaN surface was barely corroded and etched after accelerated CA testing under 6-sun illumination. In addition, the effects of pH on GaN stability under photoetching were examined. Higher H^+ concentrations led to more severe surface photoetching. Furthermore, increasing the SO_4^{2-} concentration alleviated the damage to the surface; this effect is attributed to the oxidation of SO_4^{2-} and/or HSO_4^- ions and ionic conductivity. This study provides valuable insights into the electrolyte effect on the PEC behavior of GaN and other semiconductors and can guide the selection of the appropriate working environment for PECMP.

Table 1 Onset potential, saturated photocurrent, and Ra of GaN after CA tests at different anion concentrations

Electrolyte	pH	Onset potential (V)	Saturated photocurrent (mA/cm^2)	Ra after the CA test (nm)
0.5 M Na_2SO_4	7	1.46	0.28	3.63
0.5 M H_2SO_4	0	1.18	0.38	28.4
0.5 M H_2SO_4 + 0.5 M Na_2SO_4	0	0.69	0.29	17.7
0.5 M H_2SO_4 + 1.5 M Na_2SO_4	0	0.81	0.28	12.7

Supplementary Information The online version contains supplementary material available at <https://doi.org/10.1007/s41871-024-00224-x>.

Acknowledgements This research was made possible through the support of the Southern University of Science and Technology (SUSTech) research startup grant. The authors gratefully acknowledge financial support from the Shenzhen Key Laboratory of Intelligent Robotics and Flexible Manufacturing Systems (ZDSYS20220527171403009), and the valuable technical support provided by the SUSTech Core Research Facilities and the SUSTech Energy Research Institute for Carbon Neutrality. Special thanks are given to Thermo Fisher for their technical support during the in situ Raman experiments.

Author Contributions All authors read and approved the final manuscript.

Availability of Data and Materials The authors declare that all data supporting the findings of this study are available within the article.

Declarations

Competing Interests The authors declare that they have no competing interests.

Open Access This article is licensed under a Creative Commons Attribution 4.0 International License, which permits use, sharing, adaptation, distribution and reproduction in any medium or format, as long as you give appropriate credit to the original author(s) and the source, provide a link to the Creative Commons licence, and indicate if changes were made. The images or other third party material in this article are included in the article's Creative Commons licence, unless indicated otherwise in a credit line to the material. If material is not included in the article's Creative Commons licence and your intended use is not permitted by statutory regulation or exceeds the permitted use, you will need to obtain permission directly from the copyright holder. To view a copy of this licence, visit <http://creativecommons.org/licenses/by/4.0/>.

References

- Xu Z, Tang Y, Rommel M (2020) Foreword to the special issue on wide-bandgap (WBG) semiconductors: from fundamentals to applications. *Nanotechnol Precis Eng* 3(4):187–188. <https://doi.org/10.1016/j.npe.2021.01.001>
- Kucharski R, Sochacki T, Lucznik B, Bockowski M (2020) Growth of bulk GaN crystals. *J Appl Phys* 128(5):050902. <https://doi.org/10.1063/5.0009900>
- Wang Z, Wang G, Liu X, Wang S, Wang T, Zhang S, Yu J, Zhao G, Zhang L (2021) Two-dimensional wide band-gap nitride semiconductor GaN and AlN materials: properties, fabrication and applications. *J Mater Chem C* 9(48):17201–17232. <https://doi.org/10.1039/D1TC04022G>
- He J, Cheng W-C, Wang Q, Cheng K, Yu H, Chai Y (2021) Recent advances in GaN-based power HEMT devices. *Adv Electron Mater* 7(4):2001045. <https://doi.org/10.1002/aelm.202001045>
- Shu T, Liu F, Chen S, Liu X, Zhang C, Cheng GJ (2022) Origins of ultrafast pulse laser-induced nano straight lines with potential applications in detecting subsurface defects in silicon carbide wafers. *Nanomanufacturing Metrol* 5(2):167–178. <https://doi.org/10.1007/s41871-022-00133-x>
- Huang C, Zhang H, Sun H (2020) Ultraviolet optoelectronic devices based on AlGaIn-SiC platform: towards monolithic photonics integration system. *Nano Energy* 77:105149. <https://doi.org/10.1016/j.nanoen.2020.105149>
- Kwak H, Kim J (2023) Semiconductor multilayer nanometrology with machine learning. *Nanomanufacturing Metrol* 6(1):15. <https://doi.org/10.1007/s41871-023-00193-7>
- Zhao L (2020) Surface defects in 4H-SiC homoepitaxial layers. *Nanotechnol Precis Eng* 3(4):229–234. <https://doi.org/10.1016/j.npe.2020.12.001>
- Zhang J, Dong P, Dang K, Zhang Y, Yan Q, Xiang H, Su J, Liu Z, Si M, Gao J, Kong M, Zhou H, Hao Y (2022) Ultra-wide bandgap semiconductor Ga₂O₃ power diodes. *Nat Commun* 13(1):3900. <https://doi.org/10.1038/s41467-022-31664-y>
- Meneghesso G, Meneghini M, Zanoni E (2018) Gallium nitride-enabled high frequency and high efficiency power conversion. SpringerLink. <https://doi.org/10.1007/978-3-319-77994-2Link>
- Meneghini M, Meneghesso G, Zanoni E (2017) Power GaN devices: materials, applications and reliability. SpringerLink. <https://doi.org/10.1007/978-3-319-43199-4>
- Qi Y, Wang D, Zhou J, Zhang K, Kong Y, Wu S, Chen T (2020) Effect of x-ray irradiation on threshold voltage of AlGaIn/GaN HEMTs with p-GaN and MIS gates. *Nanotechnol Precis Eng* 3(4):241–243. <https://doi.org/10.1016/j.npe.2020.11.001>
- Zhang Z, Xu Z, Song Y, Liu T, Dong B, Liu J, Wang H (2021) Interfacial stress characterization of GaN epitaxial layer with sapphire substrate by confocal Raman spectroscopy. *Nanotechnol Precis Eng* 4(2):023002. <https://doi.org/10.1063/1.50003818>
- Zeng G, Pham TA, Vanka S, Liu G, Song C, Cooper JK, Mi Z, Ogitsu T, Toma FM (2021) Development of a photoelectrochemically self-improving Si/GaN photocathode for efficient and durable H₂ production. *Nat Mater* 20(8):1130–1135. <https://doi.org/10.1038/s41563-021-00965-w>
- Zhou P, Navid IA, Ma Y, Xiao Y, Wang P, Ye Z, Zhou B, Sun K, Mi Z (2023) Solar-to-hydrogen efficiency of more than 9% in photocatalytic water splitting. *Nature* 613(7942):66–70. <https://doi.org/10.1038/s41586-022-05399-1>
- Dong WJ, Xiao Y, Yang KR, Ye Z, Zhou P, Navid IA, Batista VS, Mi Z (2023) Pt nanoclusters on GaN nanowires for solar-assisted seawater hydrogen evolution. *Nat Commun* 14(1):179. <https://doi.org/10.1038/s41467-023-35782-z>
- Wang K, Sheng C (2020) Application of GaN in 5G Technology. *J Phys Conf Ser* 1699(1):012004. <https://doi.org/10.1088/1742-6596/1699/1/012004>
- Shen B (2015) Development trends of GaN-based wide band-gap semiconductors: from solid state lighting to power electronic devices. *Front Optoelectron* 8(4):456–460. <https://doi.org/10.1007/s12200-015-0459-1>
- Huang C, Zhang Z, Wang X, Liu H, Zhang G (2023) An MMIC LNA for millimeter-wave radar and 5G applications with GaN-on-SiC technology. *Sensors* 23(14):6611. <https://doi.org/10.3390/s23146611>
- Ajayan J, Nirmal D, Ramesh R, Bhattacharya S, Tayal S, Leo Joseph LMI, Raju Thoutam L, Ajitha D (2021) A critical review of AlGaIn/GaN-heterostructure based Schottky diode/HEMT hydrogen (H₂) sensors for aerospace and industrial applications. *Measurement* 186:110100. <https://doi.org/10.1016/j.measurement.2021.110100>
- Delgado Carrascon R, Richter S, Nawaz M, Paskov PP, Darakchieva V (2022) Hot-wall MOCVD for high-quality homoepitaxy of GaN: understanding nucleation and design of growth strategies. *Cryst Growth Des* 22(12):7021–7030. <https://doi.org/10.1021/acs.cgd.2c00683>
- Kirchner C, Schwegler V, Eberhard F, Kamp M, Ebeling KJ, Prystawko P, Leszczynski M, Grzegory I, Porowski S (2000) MOVPE homoepitaxy of high-quality GaN: crystal growth and devices. *Prog Cryst Growth Charact Mater* 41(1):57–83. [https://doi.org/10.1016/S0960-8974\(00\)00044-9](https://doi.org/10.1016/S0960-8974(00)00044-9)

23. Shi D, Zhou W, Zhao T (2023) Polishing of diamond, SiC, GaN based on the oxidation modification of hydroxyl radical: status, challenges and strategies. *Mater Sci Semicond Process* 166:107737. <https://doi.org/10.1016/j.mssp.2023.107737>
24. Xu L, Park K, Lei H, Liu P, Kim E, Cho Y, Kim T, Chen C (2023) Chemically-induced active micro-nano bubbles assisting chemical mechanical polishing: modeling and experiments. *Friction* 11(9):1624–1640. <https://doi.org/10.1007/s40544-022-0668-8>
25. Krishnan M, Nalaskowski JW, Cook LM (2010) Chemical mechanical planarization: slurry chemistry, materials, and mechanisms. *Chem Rev* 110(1):178–204. <https://doi.org/10.1021/cr900170z>
26. Aida H, Doi T, Takeda H, Katakura H, Kim SW, Koyama K, Yamazaki T, Uneda M (2012) Ultraprecision CMP for sapphire, GaN, and SiC for advanced optoelectronics materials. *Curr Appl Phys* 12:S41–S46. <https://doi.org/10.1016/j.cap.2012.02.016>
27. Asghar K, Qasim M, Nelabhotla DM, Das D (2016) Effect of surfactant and electrolyte on surface modification of c-plane GaN substrate using chemical mechanical planarization (CMP) process. *Colloids Surf Physicochem Eng Asp* 497:133–145. <https://doi.org/10.1016/j.colsurfa.2016.02.035>
28. Aida H, Takeda H, Kim S-W, Aota N, Koyama K, Yamazaki T, Doi T (2014) Evaluation of subsurface damage in GaN substrate induced by mechanical polishing with diamond abrasives. *Appl Surf Sci* 292:531–536. <https://doi.org/10.1016/j.apsusc.2013.12.005>
29. Wang J, Wang T, Pan G, Lu X (2016) Effect of photocatalytic oxidation technology on GaN CMP. *Appl Surf Sci* 361:18–24. <https://doi.org/10.1016/j.apsusc.2015.11.062>
30. Ou LW, Wang YH, Hu HQ, Zhang LL, Dong ZG, Kang RK, Guo DM, Shi K (2019) Photochemically combined mechanical polishing of n-type gallium nitride wafer in high efficiency. *Precis Eng* 55:14–21. <https://doi.org/10.1016/j.precisioneng.2018.08.002>
31. Pan J, Zhuo Z, Zhang Q, Zheng Q, Yan Q (2022) Friction and wear mechanisms for single crystal GaN based on an electro-Fenton enhanced chemical reaction. *Wear* 498–499:204315. <https://doi.org/10.1016/j.wear.2022.204315>
32. Aida H, Takeda H, Doi T (2021) Analysis of mechanically induced subsurface damage and its removal by chemical mechanical polishing for gallium nitride substrate. *Precis Eng* 67:350–358. <https://doi.org/10.1016/j.precisioneng.2020.10.007>
33. Zhou M, Zhong M, Xu W (2023) Novel model of material removal rate on ultrasonic-assisted chemical mechanical polishing for sapphire. *Friction* 11(11):2073–2090. <https://doi.org/10.1007/s40544-022-0713-7>
34. Zhang L, Deng H (2020) Highly efficient and damage-free polishing of GaN (0 0 0 1) by electrochemical etching-enhanced CMP process. *Appl Surf Sci* 514:145957. <https://doi.org/10.1016/j.apsusc.2020.145957>
35. Zhang L, Wu B, Zhang Y, Deng H (2023) Highly efficient and atomic scale polishing of GaN via plasma-based atom-selective etching. *Appl Surf Sci* 620:156786. <https://doi.org/10.1016/j.apsusc.2023.156786>
36. Yan J, Pan J, Yan Q, Zhou R, Wu Y (2023) Controllable electrochemical-magnetorheological finishing of single-crystal gallium nitride wafers. *J Solid State Electrochem* 27(3):597–610. <https://doi.org/10.1007/s10008-022-05322-8>
37. Wu J, Afzal B, Huang Z, Yang M, Sun S (2023) Study on new magnetorheological chemical polishing process for GaN crystals: polishing solution composition, process parameters, and roughness prediction model. *Smart Mater Struct* 32(3):035031. <https://doi.org/10.1088/1361-665X/acb86f>
38. Dong Z, Ou L, Kang R, Hu H, Zhang B, Guo D, Shi K (2019) Photoelectrochemical mechanical polishing method for n-type gallium nitride. *CIRP Ann* 68(1):205–208. <https://doi.org/10.1016/j.cirp.2019.04.121>
39. Ou L, Dong Z, Kang R, Shi K, Guo D (2019) Photoelectrochemically combined mechanical polishing of n-type gallium nitride wafer by using metal nanoparticles as photocathodes. *Int J Adv Manuf Technol* 105(11):4483–4489. <https://doi.org/10.1007/s00170-018-03279-5>
40. Qiao L, Ou L, Shi K (2023) Wireless photoelectrochemical mechanical polishing for inert compound semiconductor wafers. *J Manuf Process* 88:97–109. <https://doi.org/10.1016/j.jmapro.2023.01.039>
41. Wang J, Wang T, Pan G, Lu X (2015) Mechanism of GaN CMP Based on H₂O₂ Slurry Combined with UV Light. *ECS J Solid State Sci Technol* 4(3):P112. <https://doi.org/10.1149/2.0191503jss>
42. Shi X, Zou C, Pan G, Gong H, Xu L, Zhou Y (2017) Atomically smooth gallium nitride surface prepared by chemical-mechanical polishing with S₂O₈²⁻-Fe²⁺ based slurry. *Tribol Int* 110:441–450. <https://doi.org/10.1016/j.triboint.2016.09.037>
43. Asghar K, Qasim M, Das D (2014) Effect of polishing parameters on chemical mechanical planarization of C-Plane (0001) gallium nitride surface using SiO₂ and Al₂O₃ abrasives. *ECS J Solid State Sci Technol* 3(8):P277. <https://doi.org/10.1149/2.0181407jss>
44. Murata J, Kubota A, Yagi K, Sano Y, Hara H, Arima K, Okamoto T, Mimura H, Yamauchi K (2008) Chemical planarization of GaN using hydroxyl radicals generated on a catalyst plate in H₂O₂ solution. *J Cryst Growth* 310(7):1637–1641. <https://doi.org/10.1016/j.jcrysgro.2007.11.093>
45. Zhu Y, Niu X, Hou Z, Zhang Y, Shi Y, Wang R (2022) Effect and mechanism of oxidant on alkaline chemical mechanical polishing of gallium nitride thin films. *Mater Sci Semicond Process* 138:106272. <https://doi.org/10.1016/j.mssp.2021.106272>
46. Kayao K, Toh D, Yamauchi K, Sano Y (2023) Role of photoelectrochemical oxidation in enabling high-efficiency polishing of gallium nitride. *ECS J Solid State Sci Technol* 12(6):063005. <https://doi.org/10.1149/2162-8777/acde61>
47. Walczak MM, Dryer DA, Jacobson DD, Foss MG, Flynn NT (1997) pH dependent redox couple: an illustration of the nernst equation. *J Chem Educ* 74(10):1195. <https://doi.org/10.1021/ed074p1195>
48. Vidal-Iglesias FJ, Solla-Gullón J, Rodes A, Herrero E, Aldaz A (2012) Understanding the nernst equation and other electrochemical concepts: an easy experimental approach for students. *J Chem Educ* 89(7):936–939. <https://doi.org/10.1021/ed2007179>
49. Fang W, Fu L, Qin A, Lin Y, Xv R (2022) Highly active and self-healing co-doped BiVO₄ photoanode in borate buffer to enhance charge separation and water oxidation kinetics during photoelectrochemical water splitting. *ACS Appl Energy Mater* 5(5):6313–6323. <https://doi.org/10.1021/acsaem.2c00477>
50. Xie J, Yang P, Liang X, Xiong J (2018) Self-improvement of Ti:Fe₂O₃ photoanodes: photoelectrocatalysis improvement after long-term stability testing in alkaline electrolyte. *ACS Appl Energy Mater* 1(6):2769–2775. <https://doi.org/10.1021/acsaem.8b00445>
51. Feng C, Wang F, Liu Z, Nakabayashi M, Xiao Y, Zeng Q, Fu J, Wu Q, Cui C, Han Y, Shibata N, Domen K, Sharp ID, Li Y (2021) A self-healing catalyst for electrocatalytic and photoelectrochemical oxygen evolution in highly alkaline conditions. *Nat Commun* 12(1):5980. <https://doi.org/10.1038/s41467-021-26281-0>
52. Tseng WJ, van Dorp DH, Lieten RR, Mehta B, Vereecken PM, Borghs G (2013) Enhanced photocatalytic activity of nanoroughened GaN by dry etching. *ECS Electrochem Lett* 2(11):H51. <https://doi.org/10.1149/2.012311eel>
53. Baker DR, Lundgren CA (2017) Electrochemical determination of the gallium-nitride photocorrosion potential in acidic media. *J Mater Chem A* 5(39):20978–20984. <https://doi.org/10.1039/C7TA04545J>

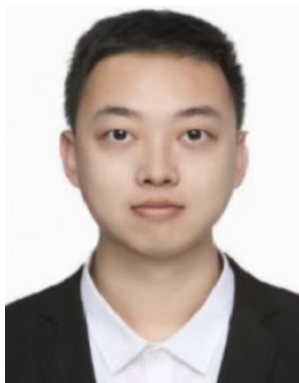
54. Bardwell JA, Webb JB, Tang H, Fraser J, Moisa S (2001) Ultra-violet photoenhanced wet etching of GaN in $K_2S_2O_8$ solution. *J Appl Phys* 89(7):4142–4149. <https://doi.org/10.1063/1.1352684>
55. Son H, Park JH, Uthirakumar P, Kuznetsov AY, Lee I-H (2020) Impact of chloride surface treatment on nano-porous GaN structure for enhanced water-splitting efficiency. *Appl Surf Sci* 532:147465. <https://doi.org/10.1016/j.apsusc.2020.147465>
56. Kim H, Bae H, Bang SW, Kim S, Lee SH, Ryu S-W, Ha J-S (2019) Enhanced photoelectrochemical stability of GaN photoelectrodes by Al_2O_3 surface passivation layer. *Opt Express* 27(4):A206–A215. <https://doi.org/10.1364/OE.27.00A206>
57. Tseng WJ, van Dorp DH, Lieten RR, Vereecken PM, Borghs G (2014) Anodic etching of n-GaN epilayer into porous GaN and its photoelectrochemical properties. *J Phys Chem C* 118(51):29492–29498. <https://doi.org/10.1021/jp508314q>
58. Schwab MJ, Chen D, Han J, Pfefferle LD (2013) Aligned mesopore arrays in GaN by anodic etching and photoelectrochemical surface etching. *J Phys Chem C* 117(33):16890–16895. <https://doi.org/10.1021/jp401890d>
59. Al-Heuseen K, Hashim MR, Ali NK (2011) Effect of different electrolytes on porous GaN using photo-electrochemical etching. *Appl Surf Sci* 257(14):6197–6201. <https://doi.org/10.1016/j.apsusc.2011.02.031>
60. Chen S, Wang L-W (2012) Thermodynamic oxidation and reduction potentials of photocatalytic semiconductors in aqueous solution. *Chem Mater* 24(18):3659–3666. <https://doi.org/10.1021/cm302533s>
61. Nandjou F, Haussener S (2019) Kinetic competition between water-splitting and photocorrosion reactions in photoelectrochemical devices. *Chemsuschem* 12(9):1984–1994. <https://doi.org/10.1002/cssc.201802558>
62. Pal Y, Anthony Raja M, Madhumitha M, Nikita A, Neethu A (2021) Fabrication and characterization of gallium nitride thin film deposited on a sapphire substrate for photoelectrochemical water splitting applications. *Optik* 226:165410. <https://doi.org/10.1016/j.ijleo.2020.165410>
63. Thapa J, Liu B, Woodruff SD, Chorpene BT, Buric MP (2017) Raman scattering in single-crystal sapphire at elevated temperatures. *Appl Opt* 56(31):8598–8606. <https://doi.org/10.1364/AO.56.008598>
64. Hushur A, Manghnani MH, Narayan J (2009) Raman studies of GaN/sapphire thin film heterostructures. *J Appl Phys* 106(5):054317. <https://doi.org/10.1063/1.3213370>
65. Cao D, Xiao H, Gao Q, Yang X, Luan C, Mao H, Liu J, Liu X (2017) Fabrication and improved photoelectrochemical properties of a transferred GaN-based thin film with InGaN/GaN layers. *Nanoscale* 9(32):11504–11510. <https://doi.org/10.1039/C7NR03622A>
66. Jeffries AM, Ding L, Williams JJ, Williamson TL, Hoffbauer MA, Honsberg CB, Bertoni MI (2017) Gallium nitride grown by molecular beam epitaxy at low temperatures. *Thin Solid Films* 642:25–30. <https://doi.org/10.1016/j.tsf.2017.07.066>
67. He W, Wu W, Li Q, Chen K, Lu X (2020) Facile fabrication of Ga_2O_3 nanorods for photoelectrochemical water splitting. *Chem-NanoMat* 6(2):208–211. <https://doi.org/10.1002/cnma.201900583>
68. Gao YH, Bando Y, Sato T, Zhang YF, Gao XQ (2002) Synthesis, Raman scattering and defects of β - Ga_2O_3 nanorods. *Appl Phys Lett* 81(12):2267–2269. <https://doi.org/10.1063/1.1507835>
69. Jalilian R, Yazdanpanah MM, Pradhan BK, Sumanasekera GU (2006) Crystalline nano-structures of Ga_2O_3 with herringbone morphology. *Chem Phys Lett* 426(4):393–397. <https://doi.org/10.1016/j.cplett.2006.05.089>
70. Hill JC, Choi K-S (2012) Effect of electrolytes on the selectivity and stability of n-type WO_3 photoelectrodes for use in solar water oxidation. *J Phys Chem C* 116(14):7612–7620. <https://doi.org/10.1021/jp209909b>
71. Fujii K, Ohkawa K (2006) Bias-assisted H_2 gas generation in HCl and KOH solutions using n-type GaN photoelectrode. *J Electrochem Soc* 153(3):A468. <https://doi.org/10.1149/1.2161572>
72. Kamimura J, Bogdanoff P, Abdi FF, Lähnemann J, van de Krol R, Riechert H, Geelhaar L (2017) Photoelectrochemical properties of GaN photoanodes with cobalt phosphate catalyst for solar water splitting in neutral electrolyte. *J Phys Chem C* 121(23):12540–12545. <https://doi.org/10.1021/acs.jpcc.7b02253>
73. Huygens IM, Strubbe K, Gomes WP (2000) Electrochemistry and photoetching of n-GaN. *J Electrochem Soc* 147(5):1797. <https://doi.org/10.1149/1.1393436>
74. Parvin M, Petrulevičienė M, Savickaja I, Šebeka B, Karpicz R, Grigucevičienė A, Ramanauskas R, Juodkazytė J (2022) Influence of morphology on photoanodic behaviour of WO_3 films in chloride and sulphate electrolytes. *Electrochim Acta* 403:139710. <https://doi.org/10.1016/j.electacta.2021.139710>
75. Benton J, Bai J, Wang T (2013) Enhancement in solar hydrogen generation efficiency using a GaN-based nanorod structure. *Appl Phys Lett* 102(17):173905. <https://doi.org/10.1063/1.4803926>
76. Yu J, Dai Y, He Q, Zhao D, Shao Z, Ni M (2021) A mini-review of noble-metal-free electrocatalysts for overall water splitting in non-alkaline electrolytes. *Mater Rep Energy* 1(2):100024. <https://doi.org/10.1016/j.matre.2021.100024>
77. Xie X, Du L, Yan L, Park S, Qiu Y, Sokolowski J, Wang W, Shao Y (2022) Oxygen evolution reaction in alkaline environment: material challenges and solutions. *Adv Funct Mater* 32(21):2110036. <https://doi.org/10.1002/adfm.202110036>
78. Liang Q, Brocks G, Bieberle-Hütter A (2021) Oxygen evolution reaction (OER) mechanism under alkaline and acidic conditions. *J Phys Energy* 3(2):026001. <https://doi.org/10.1088/2515-7655/abdc85>
79. Ding C, Zhou X, Shi J, Yan P, Wang Z, Liu G, Li C (2015) Abnormal effects of cations (Li^+ , Na^+ , and K^+) on photoelectrochemical and electrocatalytic water splitting. *J Phys Chem B* 119(8):3560–3566. <https://doi.org/10.1021/acs.jpcc.5b00713>
80. Koike K, Yamamoto K, Ohara S, Kikitsu T, Ozasa K, Nakamura S, Sugiyama M, Nakano Y, Fujii K (2017) Effects of NiO-loading on n-type GaN photoanode for photoelectrochemical water splitting using different aqueous electrolytes. *Int J Hydrog Energy* 42(15):9493–9499. <https://doi.org/10.1016/j.ijhydene.2016.12.141>
81. Sreedhar A, Reddy IN, Hoai Ta QT, Cho E, Noh J-S (2019) Insight into anions and cations effect on charge carrier generation and transportation of flake-like Co-doped ZnO thin films for stable PEC water splitting activity. *J Electroanal Chem* 855:113583. <https://doi.org/10.1016/j.jelechem.2019.113583>
82. Shinagawa T, Takanabe K (2017) Towards versatile and sustainable hydrogen production through electrocatalytic water splitting: electrolyte engineering. *Chemsuschem* 10(7):1318–1336. <https://doi.org/10.1002/cssc.201601583>
83. Nakajima T, Kanaori M, Hagino A, Tateno H, Tsuchiya T, Sayama K (2018) Sustainable chromic acid oxidation: solar-driven recycling of hexavalent chromium ions for quinone production by WO_3 nanosponge photoanodes. *J Mater Chem A* 6(1):110–117. <https://doi.org/10.1039/C7TA08001H>
84. Wang T, Gong J (2017) Overestimated solar water splitting performance on oxide semiconductor anodes. *Sci China Mater* 60(1):90–92. <https://doi.org/10.1007/s40843-016-5158-0>
85. Liu J, Zou Y, Jin B, Zhang K, Park JH (2019) Hydrogen peroxide production from solar water oxidation. *ACS Energy Lett* 4(12):3018–3027. <https://doi.org/10.1021/acsenerylett.9b02199>
86. Fuku K, Wang N, Miseki Y, Funaki T, Sayama K (2015) Photoelectrochemical reaction for the efficient production of hydrogen and high-value-added oxidation reagents. *Chemsuschem* 8(9):1593–1600. <https://doi.org/10.1002/cssc.201403463>

87. Yang S, Liu Y, Sun C (2006) Preparation of anatase TiO₂/Ti nano-tube-like electrodes and their high photoelectrocatalytic activity for the degradation of PCP in aqueous solution. *Appl Catal Gen* 301(2):284–291. <https://doi.org/10.1016/j.apcata.2005.12.016>
88. Lee Y, Khim J (2021) Effects of electrolyte concentration and anion identity on photoelectrochemical degradation of phenol: focusing on the change at the photoanode/solution interface. *J Environ Chem Eng* 9(6):106717. <https://doi.org/10.1016/j.jece.2021.106717>
89. Chen X, Chen R, Zhu X, Liao Q, Zhang Y, Ye D, Zhang B, Yu Y, Li J (2019) A solar responsive cubic nanosized CuS/Cu₂O/Cu photocathode with enhanced photoelectrochemical activity. *J Catal* 372:182–192. <https://doi.org/10.1016/j.jcat.2019.02.031>

Publisher's Note Springer Nature remains neutral with regard to jurisdictional claims in published maps and institutional affiliations.



Huiqiang Liang received the BS degree in new energy materials and devices from Guangdong University of Technology in 2022. Now, he is pursuing his MS degree in Southern University of Science and Technology. His research interests include the mechanical properties, photoelectrochemistry and mechanochemistry mechanisms of wide bandgap semiconductor materials.



Zhenghao Wei received the BS degree in Mechanical and electronic engineering from North University of China in 2023. Now, he is pursuing his MS degree in Southern University of Science and Technology. His research interests include the mechanical properties and mechanochemistry mechanism of wide bandgap semiconductor materials.



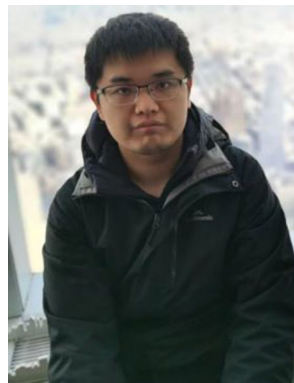
Jiongchong Fang received the BS degree in energy and power engineering from Guangdong University of Technology in 2023. Now, he is pursuing his PhD degree in Southern University of Science and Technology. His research interests include the efficient mechanical catalysts and its applications in hydrogen production.



Yanming Li is currently a PhD student at Sun Yat-sen University, China. He received his Master's degree from Sun Yat-sen University in 2022. His research mainly focuses on catalytic processes and materials for the transformation of small organic molecules to energy-related feedstocks, such as methane oxidation and carbon dioxide reduction.



Changli Li is an Associate Professor at the School of Materials, Sun Yatsen University, China. He received his PhD degree in Mechanical Engineering from the University of Tokyo, Japan, in 2015. After his Post-Doctoral studies at Tsinghua University and the University of British Columbia, he began his independent career as a faculty member at Sun Yat-sen University. His research activities focus on the synthesis of nanostructured materials and semiconductor heterojunctions for electrochemical and photoelectrochemical energy conversion.



Zhirun Xie is currently a post-doctoral research fellow in the group of Prof. Yun Hau Ng, at the Laboratory of Catalysis for Alternative & Renewable Energy, City University of Hong Kong. He received his Ph.D. degree in Chemical Engineering from the University of New South Wales (UNSW) in 2020 under the supervision of Prof. Yun Hau Ng and Prof. Jason Scott. His research interest focuses on the design of efficient photo(electro)catalysts for solar energy conversion and utilization.



Yun Hau Ng is a professor at the School of Energy and Environment, and the director of Low-Carbon and Climate Impact Research Centre (LCCIC) at City University of Hong Kong. He received his PhD from Osaka University in 2009. After brief attachment at the University of Notre Dame, he moved to Australia and became a lecturer at the University of New South Wales (UNSW) in 2014. He joined CityU in 2018. His research is focused on the development of novel photoactive

semiconductors for sunlight energy conversion, including hydrogen generation from water and conversion of carbon dioxide to solar fuels.



Guosong Zeng received the BS degree in measurement and control technology and instrumentation from Tianjin University in 2010. He received the PhD degree in mechanical engineering from Lehigh University in 2018. Since October 2021, he started the assistant professorship in Southern University of Science and Technology. His research focuses on materials tribology, mechanical properties of wide bandgap semiconductor materials, electrochemistry, photocatalysis and photoelectrochemistry.